The Astrophysical Journal, 650:1020–1027, 2006 October 20

COSMIC-RAY ACCELERATION AT ULTRARELATIVISTIC SHOCK WAVES: EFFECTS OF DOWNSTREAM SHORT-WAVE TURBULENCE

Jacek Niemiec
Department of Physics and Astronomy, Iowa State University, Ames, IA 50011; and Instytut Fizyki Jądrowej PAN, ul. Radzikowskiego 152, 31-342 Kraków, Poland; niemiec@iastate.edu

Michał Ostrowski
Obserwatorium Astronomiczne, Uniwersytet Jagielloński, ul. Orla 171, 30-244 Kraków, Poland

and

Martin Pohl
Department of Physics and Astronomy, Iowa State University, Ames, IA 50011
Received 2006 March 13; accepted 2006 June 13

ABSTRACT

The present paper is the last of a series studying the first-order Fermi acceleration processes at relativistic shock waves with the method of Monte Carlo simulations applied to shocks propagating in realistically modeled turbulent magnetic fields. The model of the background magnetic field structure of Niemiec & Ostrowski has been augmented here by a large-amplitude short-wave downstream component, imitating that generated by plasma instabilities at the shock front. Following the recent work of Niemiec & Ostrowski, we have considered ultrarelativistic shocks with the mean magnetic field oriented both oblique and parallel to the shock normal. For both cases, simulations have been performed for different choices of magnetic field perturbations, represented by various wave power spectra within a wide wave-vector range. The results show that the introduction of the short-wave component downstream of the shock is not sufficient to produce power-law particle spectra with the "universal" spectral index 4.2. On the contrary, concave spectra with cutoffs are preferentially formed, the curvature and cutoff energy being dependent on the properties of turbulence. Our results suggest that the electromagnetic emission observed from astrophysical sites with relativistic jets, e.g., active galactic nuclei and gamma-ray bursts, is likely generated by particles accelerated in processes other than the widely invoked first-order Fermi mechanism.

Subject headings: acceleration of particles — cosmic rays — gamma rays: bursts — methods: numerical — MHD — relativity — shock waves

1. INTRODUCTION

Realistic modeling of first-order Fermi cosmic-ray acceleration at relativistic shock waves is a difficult task due to the strong dependence of the resulting particle spectra on the essentially unknown local conditions at such shocks. Therefore, progress in this field mostly arises from the increasingly more realistic MHD conditions that are assumed to apply near the shocks. For mildly relativistic shocks in the *test particle* approach, the advances that have been made in the past 20 years involve a semianalytic solution of the particle pitch-angle diffusion equation at parallel shocks (Kirk & Schneider 1987), the effects of different shock compressions in parallel shocks (Heavens & Drury 1988), the impact of an oblique mean magnetic field for subluminal configurations (Kirk & Heavens 1989), and the effects of oblique field configurations at sub- and superluminal shocks considered with an increasing degree of complication, applying successively more realistic physical approximations (Ostrowski 1991, 1993; Bednarz & Ostrowski 1996; Niemiec & Ostrowski 2004). For ultrarelativistic shocks, the notion of a "universal" spectral index was first described by Bednarz & Ostrowski (1998) and later found in a variety of studies (Gallant & Achterberg 1999; Kirk et al. 2000; Achterberg et al. 2001; Lemoine & Pelletier 2003; Ellison & Double 2004), but more recent studies (Niemiec & Ostrowski 2006) indicate basic problems with first-order Fermi acceleration, in particular in generating wide-energy power-law spectra. The latter work also contains a more systematic discussion of the subject literature.

On the other hand, there have been attempts to self-consistently derive the electromagnetic shock structure. One very simplified approach applied modeling of nonlinear effects in the first-order Fermi acceleration at the shock (e.g., Ellison & Double 2002). The limitations of this technique arise from the approximate treatment of particle scattering near the shock and its simple scaling with particle energy instead of realistically accounting for the microphysics of the process. A more realistic microscopic and self-consistent description of the collisionless shock transition may be afforded by particle-in-cell (PIC) simulations (e.g., Hoshino et al. 1992; Silva et al. 2003; Nishikawa et al. 2003, 2005; Frederiksen et al. 2004; Hededal & Nishikawa 2005; Jaroschek et al. 2005), which follow the formation of a relativistic collisionless shock starting with processes acting on the plasma scale. In these simulations, one typically observes that the generation of magnetic and electric fields is accompanied by an evolution of the particle distribution function from the background plasma conditions up to highly superthermal energy scales. Although the PIC simulations provide a wealth of information on the collisionless shock structure, they are still very much limited in dynamical range, in particular for cosmic-ray particles whose energies are many orders of magnitude larger than the plasma particle energies.

The present paper is a continuation of the studies of Niemiec & Ostrowski (2004, 2006). Here we attempt to approximately incorporate the results of the PIC simulations concerning the generation of magnetic fields at relativistic shocks into the test particle Monte Carlo simulations of cosmic-ray particle acceleration.

As in the previous papers, we study ultrarelativistic shock waves propagating in a medium with a magnetic field that is perturbed over a wide range of macroscopic scales. However, we also consider an additional short-wave isotropic turbulent field component downstream of the shock, analogous to the shock-generated turbulent fields revealed by the PIC simulations. We treat the amplitude of the short-wave component as a model parameter and study the effects of the small-scale perturbations on the particle spectra and angular distributions derived in the previous work.

In what follows, $c = 1$ is the speed of light. The integration of particle trajectories is performed in the respective local plasma (upstream or downstream) rest frame, and we use indices "1" and "2" to label quantities provided in the upstream and downstream frame, respectively. We consider ultrarelativistic particles with $p = E$. We use dimensionless variables, so a particle of unit energy moving in a uniform mean upstream magnetic field B_0 has the unit maximum (for $p_\perp = E$) gyroradius $r_g(E = 1) = 1$, and the respective resonance wavevector is $k_{\rm res}(E = 1) = 2\pi$.

2. DETAILS OF THE MODELING

2.1. *Magnetic Field Structure*

As in Niemiec & Ostrowski (2004, 2006), we assume a relativistic shock wave to propagate with velocity u_1 (or the respective Lorentz factor γ_1) in the upstream medium with a uniform magnetic field $\boldsymbol{B}_0 \equiv \boldsymbol{B}_{0,1}$, inclined at an angle ψ_1 to the shock normal (along the $\boldsymbol{u}_1$ direction), superimposed on which are isotropic three-dimensional magnetic field perturbations. These perturbations are characterized with a power-law wave power spectrum $F(k) \sim k^{-q}$ that is defined in a wide wavevector range ($k_{1,\rm min}$, $k_{1,\rm max}$), where $k_{1,\rm min} = 0.0001$ and $k_{1,\rm max} = 10$. Specifically, we consider the wave spectral indices $q = 1$, describing the flat power spectrum, and $q = 5/3$ for the Kolmogorov distribution. The integral power of these perturbations is given by the (upstream) amplitude

$$\delta B = \sqrt{\int_{k_{1,\rm min}}^{k_{1,\rm max}} F(k)\,dk}, \tag{1}$$

and $\delta B/B_0$ is one of our model parameters. As described in detail in Niemiec & Ostrowski (2004, 2006), the upstream field perturbations are modeled as the superposition of static sinusoidal waves of finite amplitude. The downstream magnetic field structure, including the turbulent component, is derived as the shock-compressed upstream field, and hence the downstream turbulent magnetic field is naturally anisotropic. Our method of applying the hydrodynamical shock jump conditions (for the electron-proton plasma; Heavens & Drury 1988) preserves the continuity of the magnetic field lines across the shock. In what follows, we refer to the field component described above as the "*large-scale*" (or "*long-wave*") background field.

The other physical magnetic field component considered in the present study is the short-wave turbulence, assumed to be a result of kinetic magnetic field generation processes acting at the shock. This component, taken for simplicity to be isotropic[1] and static, is imposed on the nonuniform background magnetic field downstream of the shock. The short-wave nonlinear field perturbations are introduced with a flat spectral distribution in the wavevector range ($10k_{2,\rm max}$, $100k_{2,\rm max}$), where the shortest downstream waves are the shock-compressed shortest upstream waves:

$$k_{2,\rm max} = k_{1,\rm max} R \frac{\gamma_1}{\gamma_2}. \tag{2}$$

Here $R = u_1/u_2$ is the compression ratio in the shock rest frame, and γ_1 and γ_2 are the upstream and downstream shock Lorentz factors, respectively. The wavevector range of the small-scale turbulent component is chosen to be one decade in k apart from $k_{2,\rm max}$ to separate the influence of these perturbations on the low-energy particle motion from that exerted by the short-wave component of the large-scale background field. This choice also facilitates the use of a hybrid method for the calculation of particle trajectories (see § 2.2). Note also that the definition of the short-wave component depends on the Lorentz factor of the shock. Below, we also refer to the short-wave magnetic field component as the *shock-generated turbulence* ("sh"), to distinguish it from the large-scale background field, that exists in the upstream region and is only compressed upon passage through the shock.

In our simulations, we exclusively study the first-order Fermi acceleration process and neglect second-order processes. Therefore, the turbulent magnetic field components (both short-wave and large-scale background perturbations) can be considered to be static in the respective plasma rest frames, both upstream and downstream of the shock, and electric fields that may exist in the shock transition layer are neglected.

2.2. *Monte Carlo Simulations*

The implementation of short-wave turbulence in the Monte Carlo simulations forces us to dispense with the direct integration of the particle equations of motion in the analytically modeled magnetic field (see Niemiec & Ostrowski 2006). Instead, we resume the derivation of particle trajectories with the hybrid approach proposed in Niemiec & Ostrowski (2004). Thus, particle trajectories are directly calculated from the equations of motion in the large-scale background magnetic field only, whereas the trajectory perturbations due to the shock-generated small-scale turbulence are accounted for through a small-amplitude pitch-angle scattering term. Auxiliary simulations have been performed to determine the scattering amplitude distributions for various particle energies. In the scattering procedure, after each time step Δt, the particle momentum direction is perturbed by a small angle $\Delta\Omega$. The time step itself scales with particle energy (or gyroradius), $\Delta t \propto E$, and is chosen so that the condition $c\Delta t \gg \lambda_{\rm sh}$ is always fulfilled ($\lambda_{\rm sh}$ is the wavelength of shock-generated perturbations), which means that the auxiliary simulations follow the particle scattering on the shock-generated turbulence well into the diffusive regime. Therefore, the scattering amplitude distributions also scale linearly with the short-wave turbulence amplitude, and the mean scattering angle is related to the particle energy as $\Delta\bar{\Omega} \propto E^{-1/2}$.

An individual simulation run is performed as follows. We start by injecting monoenergetic particles (with the initial energy $E_0 = 0.1$) at random positions along the shock front, with their momenta isotropically distributed within a cone around the shock normal pointing upstream of the shock. In an initial simulation cycle, the injection process is continued until the required number of particles, N, has been selected—those that after being injected upstream and then transmitted downstream

[1] Theoretical considerations by Medvedev & Loeb (1999) and numerical PIC simulations (e.g., Silva et al. 2003; Nishikawa et al. 2003; Frederiksen et al. 2004) show that the relativistic two-stream (Weibel-like) instability at the relativistic collisionless shock front leads to the generation of a strong, small-scale turbulent field downstream, that is predominantly transversal (two-dimensional) and lies in the plane of the shock. Because the magnetic field in the nonlinear regime of the two-stream instability is sustained by the structure of the ion current channels, instabilities in the ion filaments (e.g., kink and/or firehose instability) should ultimately lead to the three-dimensional turbulent magnetic field.

of the shock, succeed in recrossing the shock front again. Then the calculation of individual particle trajectories proceeds through all subsequent upstream-downstream cycles. In each cycle, a fraction of the particles escapes through a free-escape boundary introduced "far downstream" of the shock, i.e., at a location from which there is only a negligible chance that particles crossing the boundary would return back to the shock. To the particles remaining in the simulations, the trajectory-splitting procedure is applied (see Niemiec & Ostrowski 2004), so the number of particles remains constant in the acceleration process, but the statistical weights of the particles are appropriately reduced. The final spectra and angular distributions of accelerated particles, derived in the shock normal rest frame for particles crossing the shock front, are averaged over many statistically different simulation runs.

3. RESULTS

Because of the limited capabilities of present-day computers, the long-time nonlinear development of plasma instabilities leading to the generation of the short-wave turbulent downstream magnetic field component cannot yet be fully investigated, in particular for electron-ion plasma collision fronts. Therefore, the ultimate structure of the small-scale field and the global effectiveness of the generation mechanism remain uncertain. To estimate the role of the shock-generated turbulence in cosmic-ray acceleration at ultrarelativistic shocks, we introduce the small-scale wave component as isotropic three-dimensional magnetic field perturbations and treat the amplitude of these perturbations as a model parameter.

The spectra of accelerated particles for oblique superluminal shocks are presented in Figures 1–4, and those for parallel shocks are displayed in Figures 6 and 8. The amplitude of the short-wave component, $\delta B_{\rm sh}/\langle B_2\rangle$, as provided in the figures, is measured in units of the average downstream perturbed magnetic field strength $\langle B_2\rangle = \langle (\boldsymbol{B}_{0,2} + \delta \boldsymbol{B}_2)^2\rangle^{1/2}$. The spectra presented with solid lines has been derived in the turbulence model without the $\delta B_{\rm sh}$ term (most of them are presented in Niemiec & Ostrowski 2006). Some of the energetic particle distributions follow a power law in a certain energy range. In these cases, linear fits to the power-law portions of the spectra are presented, and values of the phase-space spectral indices, α, are given (the equivalent momentum distribution $dN/dp \propto p^{-\sigma}$, spectral index $\sigma = \alpha - 2$). The spectral indices may help to make a quantitative comparison of the spectra, but care must be exercised, because the spectral indices depend on the energy range chosen for the fit on account of the curvature in most of the spectra.

3.1. *Oblique Superluminal Shocks*

As shown in Niemiec & Ostrowski (2006), in the presence of the long-wave magnetic field perturbations only the first-order Fermi process at superluminal shock waves is inefficient for high-γ shocks. This is because of compression of the perturbed magnetic field at the shock which effectively produces two-dimensional field perturbations downstream, perpendicular to the shock normal. In such anisotropic turbulence, the transport of downstream particles back to the shock by means of cross-field diffusion (along the shock normal) is inefficient, but required for continuing the acceleration process. In effect, accelerated particles are advected with the general downstream plasma flow, and the resulting particle spectra are steep and/or exhibit energy cutoffs within the resonance energy range, below $E_{\rm res,max} \simeq 2\pi/k_{\rm min}$.

Accelerated particle spectra for oblique superluminal shocks in the presence of downstream short-wave shock-generated turbulence are presented in Figures 1–3 for $\psi_1 = 45^\circ$ ($u_1/\cos\psi_1 \approx 1.4c$), and in Figure 4 for $\psi_1 = 90^\circ$ (perpendicular shock). One can see that increasing the amplitude of the shock-generated turbulence leads to a more efficient acceleration with particle spectral tails extending to higher energies. However, in all cases in which $\delta B_{\rm sh}/\langle B_2\rangle \gg 1$, the energetic spectral tails are convex, so the spectral index increases with particle energy. In addition, all the spectra have cutoffs at an energy for which the resonance condition for interactions with the long-wave turbulence is still fulfilled. These features result from the fact that the influence on particle trajectories of the shock-generated small-scale turbulence decreases with increasing particle energy, and eventually becomes smaller than the influence of the large-scale background field. In our numerical approach, this corresponds to a reduction of the scattering amplitude $\Delta\Omega(E)$ (see § 2.2).

Most published studies of the first-order Fermi acceleration at ultrarelativistic shocks that apply the pitch-angle diffusion approximation (Bednarz & Ostrowski 1998; Gallant & Achterberg 1999; Kirk et al. 2000; Achterberg et al. 2001; Ellison & Double 2004; Keshet & Waxman 2005) assume scattering conditions that do not change with particle energy. As discussed by Ostrowski & Bednarz (2002), these authors show that if the small-angle scattering dominates over the possible influence of the oblique mean magnetic field component and/or the long-wave perturbations in shaping the particle trajectories, then a power-law particle distribution with the "universal" spectral index $\alpha_u \approx 4.2$ may be formed. With the more realistic magnetic field model considered in the present paper, it is not possible to reproduce these results. Here the particle spectra can approach a power-law form only in a limited energy range near the particle injection energy, as demonstrated by the fits to the low-energy parts of the spectra in Figures 1–4. The energy ranges for these fits are arbitrarily selected, but have the same low-energy bound. Note that in the figures the spectral indices, although dependent on the background conditions, are *always* larger than α_u. If one chose higher energies to derive a power-law fit to the spectra, one would obtain a larger spectral index on account of the convex shapes of the spectra. To further investigate this behavior we performed the following test using particular *unphysical* scattering conditions. We have recalculated the spectrum for $\delta B_{\rm sh}/\langle B_2\rangle = 80$ in Figure 1 (*filled circles*) for a fixed scattering amplitude at particle energies $E \geq 16$ [$\Delta\Omega(E \geq 16) = \Delta\Omega(E = 16) = {\rm const} \ll 1$]. Then the isotropic pitch-angle scattering term dominates over the long-wave or uniform field components downstream of the shock *also* at high particle energies. It enables efficient particle diffusion back to the shock, across the predominantly perpendicular large-scale magnetic field structure, and provides scattering conditions that do not change with particle energy. As a result, a power-law energy spectrum can form over a wide energy range, without a steepening or a cutoff. The spectral index $\alpha > \alpha_u$ is essentially determined by the inclination of the spectrum at an energy beyond which the scattering angle has been fixed.

In the case of superluminal shocks, the particle spectra calculated for a high amplitude of shock-generated turbulence, $\delta B_{\rm sh}/\langle B_2\rangle = 50$ in Figures 1–4, depend only weakly on the background large-scale magnetic field structure, in contrast to the $\delta B_{\rm sh} = 0$ limit (see also Niemiec & Ostrowski 2006). The acceleration process is only slightly more efficient in the case of a large amplitude of long-wave perturbations ($\delta B/B_0 = 1.0$ in Figs. 1 and 2) in which the spectral tails extend to marginally higher energies and show softer cutoffs when compared to the cases with $\delta B/B_0 = 0.3$ (Figs. 3 and 4). There are also only minor differences between the spectra derived for a flat spectrum of background perturbations, for which the wave power is uniformly

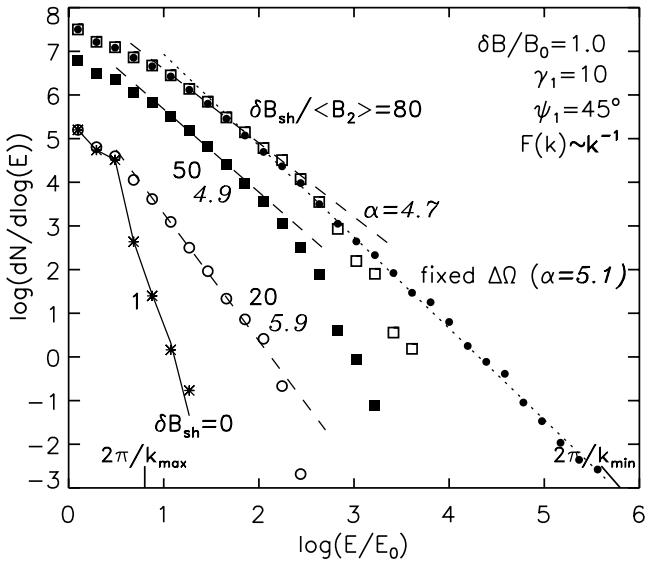

FIG. 1.—Accelerated particle spectra at oblique superluminal shocks with $\gamma_1 = 10$, $\psi_1 = 45^\circ$, and a flat wave-power spectrum of large-scale background magnetic field turbulence. The amplitude of the upstream field perturbations is $\delta B/B_0 = 1.0$. The amplitudes of the downstream shock-generated turbulence, $\delta B_{\rm sh}/\langle B_2\rangle$, are given near the respective spectra. Linear fits to some spectra are also presented with dashed lines. The energy ranges selected for the fits have the same low-energy bounds to facilitate comparison of the spectral indices α, given in italics. The spectrum plotted with a solid line applies to the case without short-wave shock-generated perturbations. The spectrum shown with filled circles is calculated with a fixed scattering term for $E \geq 16$, and the linear fit to the part of this spectrum above $E \geq 16$ is presented with a dotted line. Some spectra are vertically shifted for clarity. Particles in the energy range $(2\pi/k_{\rm max}, 2\pi/k_{\rm min})$ can satisfy the resonance condition $k_{\rm res} = 2\pi/r_g(E)$ for some of the waves in the background turbulence spectrum.

distributed per logarithmic wavevector range, and for the Kolmogorov distribution, for which most power is carried by long waves. In the latter case, one finds power-law particle spectra in a slightly wider energy range than in the case of flat distributions (compare Figs. 1 and 2 and spectra in Fig. 4), but the high-energy

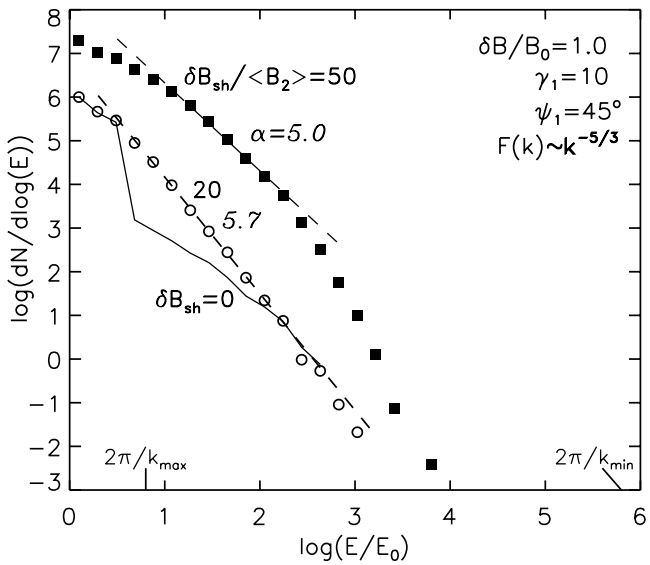

FIG. 2.—Particle spectra derived for oblique superluminal shocks for different amplitudes of shock-generated turbulence. For all spectra $\gamma_1 = 10$, $\psi_1 = 45^\circ$, and a Kolmogorov power spectrum of background long-wave turbulence with $\delta B/B_0 = 1.0$ has been assumed. The spectrum shown with the solid line is derived in the limit $\delta B_{\rm sh} = 0$ (see Fig. 2 in Niemiec & Ostrowski 2006).

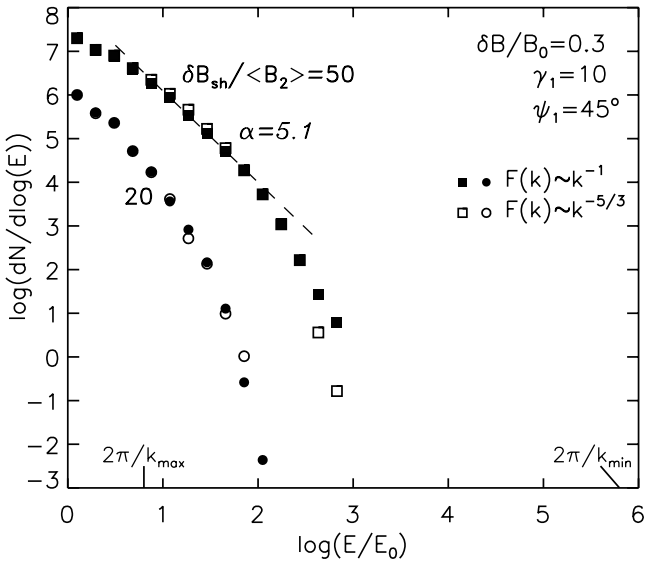

FIG. 3.—Particle spectra at superluminal ($\gamma_1 = 10$, $\psi_1 = 45^\circ$) shocks with $\delta B/B_0 = 0.3$. Filled and open symbols refer to results for a flat and a Kolmogorov wave-power spectrum of large-scale background field perturbations, respectively. The linear fit to the spectrum for the *flat* wave power spectrum is derived in an energy range with the same low-energy bound as used for the fits shown in Figs. 1 and 2.

tails and the cutoff shape remain nearly the same for both types of the wave power spectra.

The structure of the background large-scale magnetic field can, however, influence particle spectra for smaller amplitudes of the short-wave turbulence. As one can see in Figure 2, the power-law part of the spectrum for $\delta B_{\rm sh}/\langle B_2\rangle = 20$ and the Kolmogorov-type turbulence spectrum, although steeper, continues to higher energies than that for $\delta B_{\rm sh}/\langle B_2\rangle = 50$. This behavior is caused by high-amplitude long-wave background perturbations occasionally providing local scattering conditions at the shock that enable acceleration up to higher particle energies (see, e.g., the spectrum for $\delta B_{\rm sh} = 0$ in Fig. 2). This is not the case for either a flat spectrum (Fig. 1) or a small amplitude (Fig. 3) of long-wave turbulence, since in superluminal shocks, particle acceleration

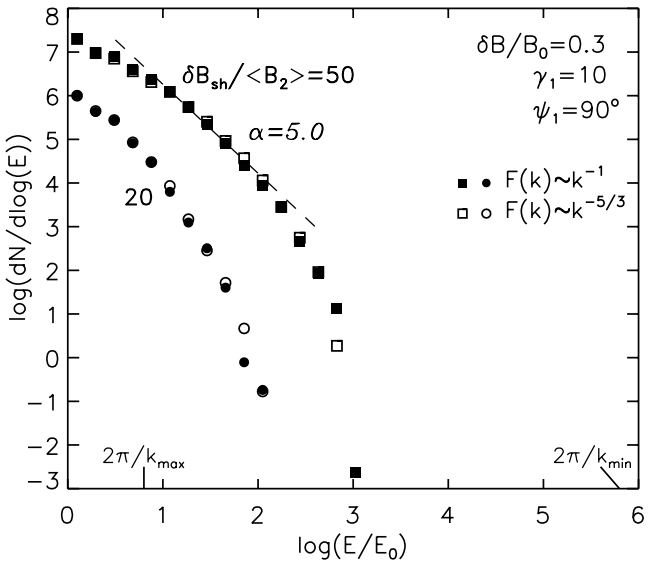

FIG. 4.—Particle spectra at perpendicular ($\gamma_1 = 10$, $\psi_1 = 90^\circ$) shocks for the same parameter combinations as in Fig. 3.

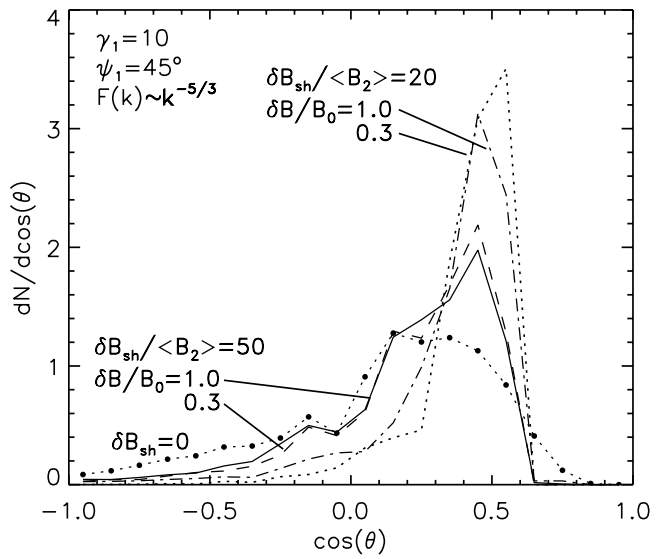

FIG. 5.—Normalized particle angular distributions as measured in the shock rest frame for superluminal shock waves with $\gamma_1 = 10$, $\psi_1 = 45^\circ$, and a Kolmogorov wave power spectrum of large-scale background magnetic field perturbations. Particles with $\cos\theta < 0$ are directed upstream of the shock. The distributions are calculated by summing the quantity $w/(|v_x| + 0.005)$ in the respective $\cos\theta$ bins at every particle shock crossing, where θ is the angle between the particle momentum and the shock normal, v_x is the normal component of the particle velocity, and w is the statistical weight of the particle. Only particles with $E \geq 1$ are included, and low-energy particles with large weights contribute most to the distributions. The angular distribution presented with filled circles is derived without short-wave perturbations ($\delta B_{\rm sh} = 0$) and for $\delta B/B_0 = 1.0$. The distributions for $\delta B_{\rm sh}/\langle B_2\rangle = 50$, and for $\delta B/B_0 = 1.0$ and 0.3 are presented with solid and dashed lines, respectively, and for $\delta B_{\rm sh}/\langle B_2\rangle = 20$, and $\delta B/B_0 = 1.0$ and 0.3 with dash-dotted and dotted lines, respectively.

processes in the absence of large-amplitude long-wave magnetic field perturbations do not produce the power-law particle spectra (Begelman & Kirk 1990; Niemiec & Ostrowski 2004, 2006).

Figure 5 presents particle angular distributions for superluminal shocks ($\psi_1 = 45^\circ$) with the Kolmogorov power spectrum of large-scale magnetic field perturbations. Note a nonmonotonic variation of the angular distributions with growing power in the small-scale turbulence, $\delta B_{\rm sh}/\langle B_2\rangle = 0$, 20, and 50. As for the low-energy particle spectra, the distributions for $\delta B_{\rm sh}/\langle B_2\rangle = 50$ do not depend on either the amplitude of the background field perturbations, or on their wave power spectrum (distributions for the flat wave power spectrum are not shown for presentation clarity). The similarity in shape of these distributions to the angular distribution derived without the $\delta B_{\rm sh}$ scattering term is caused by efficient particle scattering on the downstream short-wave perturbations at low particle energies in these cases and the occurrence of the locally subluminal conditions at the shock in the model with $\delta B_{\rm sh} = 0$ that enable a considerable fraction of downstream particles to return upstream of the shock. Note that the low-energy particle population in the model with $\delta B_{\rm sh} = 0$ (Fig. 2) that is produced in a process of "superadiabatic" particle compression at the shock (for details, see Niemiec & Ostrowski 2006) does not contribute to the angular distribution shown in Figure 5, since only particles with $E \geq 1$ are included in the distributions presented. The difference in the distributions for the smaller short-wave amplitude, $\delta B_{\rm sh}/\langle B_2\rangle = 20$, illustrates the effects the long-wave field perturbations have on the particle acceleration process, as discussed above.

A caveat is in order concerning the low-energy part of the simulated spectra. In our simulations with large-amplitude short-wave turbulence, the scattering amplitudes for low particle energies, $E \leq 1$ for the spectra with $\delta B_{\rm sh}/\langle B_2\rangle = 50$ and $E \leq 5$ for $\delta B_{\rm sh}/\langle B_2\rangle = 80$, violate the pitch-angle diffusion requirement $\Delta\Omega \ll 1$. This is because in our approach, the time between subsequent scatterings is fixed for a given particle energy, and the scattering angle scales linearly with $\delta B_{\rm sh}$ (see § 2.2), providing larger scattering amplitudes for larger values of $\langle B_2\rangle$. Therefore, the simulated spectra may suffer a weak systematic flattening at low energies.

3.2. *Parallel Shocks*

As discussed by Ostrowski & Bednarz (2002), the particle spectra with "universal" slope have been derived in effective conditions equivalent to a parallel ($\psi_1 = 0^\circ$) mean shock configuration. However, in our earlier work (Niemiec & Ostrowski 2004, 2006), we have demonstrated that the spectra formed at parallel relativistic shocks depend substantially on background conditions, and features such as a relation between the spectral index and the turbulence amplitude or a cutoff formation in the case of ultrarelativistic shocks can be observed. In this section, we investigate the role of shock-generated downstream turbulence in particle acceleration at parallel shocks. For that purpose, we have performed simulations for highly relativistic shock waves with Lorentz factors $\gamma_1 = 10$ and 30, as presented in Figures 6 and 8, respectively. For parallel shocks, the amplitude of the compressed background field downstream of the shock, $\langle B_2\rangle$, is on average much smaller than for the oblique shocks discussed in § 3.1. Therefore, the numerical constraints are largely relaxed, and we can use larger values of $\delta B_{\rm sh}/\langle B_2\rangle$, up to 300 or even 500. However, as explained in § 3.1, we would still slightly violate the pitch-angle scattering approximation at $E \leq 1$ for the spectra with $\delta B_{\rm sh}/\langle B_2\rangle = 80$ in Figures 6*a* and 6*b*, and $\delta B_{\rm sh}/\langle B_2\rangle = 300$ in Figures 6*c* and 6*d*.

Figures 6*a* and 6*b* show the results for shocks with $\gamma_1 = 10$ and large-amplitude background field perturbations ($\delta B/B_0 = 1.0$). The qualitative similarity of the spectral features observed in this case and for oblique superluminal shocks is apparent (see also Niemiec & Ostrowski 2006); the spectra are convex and display cutoffs occurring much below $E_{\rm res,max}$. This behavior proves that the large-amplitude long-wave perturbations locally form superluminal conditions at the shock, thus leading to the spectral cutoff as the pitch-angle scattering term, due to the downstream shock-generated turbulence, substantially decreases with growing particle energy. Note that in the case of a lower amplitude of the short-wave component, $\delta B_{\rm sh}/\langle B_2\rangle = 20$, the large-scale background turbulence with the Kolmogorov distribution provides acceleration conditions allowing for the formation of a quasi–power-law spectrum in a slightly wider energy range than for larger $\delta B_{\rm sh}/\langle B_2\rangle$ (Fig. 6*b*), again in correspondence with the analogous result for the superluminal shocks (Fig. 2).

For the smaller amplitude of the long-wave magnetic field perturbations, $\delta B/B_0 = 0.3$, the role of the longest perturbations is less significant, and the scattering on the short-wave turbulence can dominate up to energies higher than the upper resonance energy $E_{\rm res,max}$. This behavior can be observed in the case of the flat-spectrum large-scale background turbulence shown in Figure 6*c*. Although gradually weakening with growing particle energy, the pitch-angle diffusion term dominates over scattering by the long-wave perturbations. The scattering mean free path along the mean background magnetic field (≡ shock normal) and, correspondingly, the mean acceleration timescale increase with particle energy, but the particle spectra retain a power-law form up to the highest energies $E \approx E_{\rm res,max}$ studied in our simulations. However, the spectra are steeper than the expected "universal" spectrum, $\alpha > \alpha_u$, and only weakly dependent on

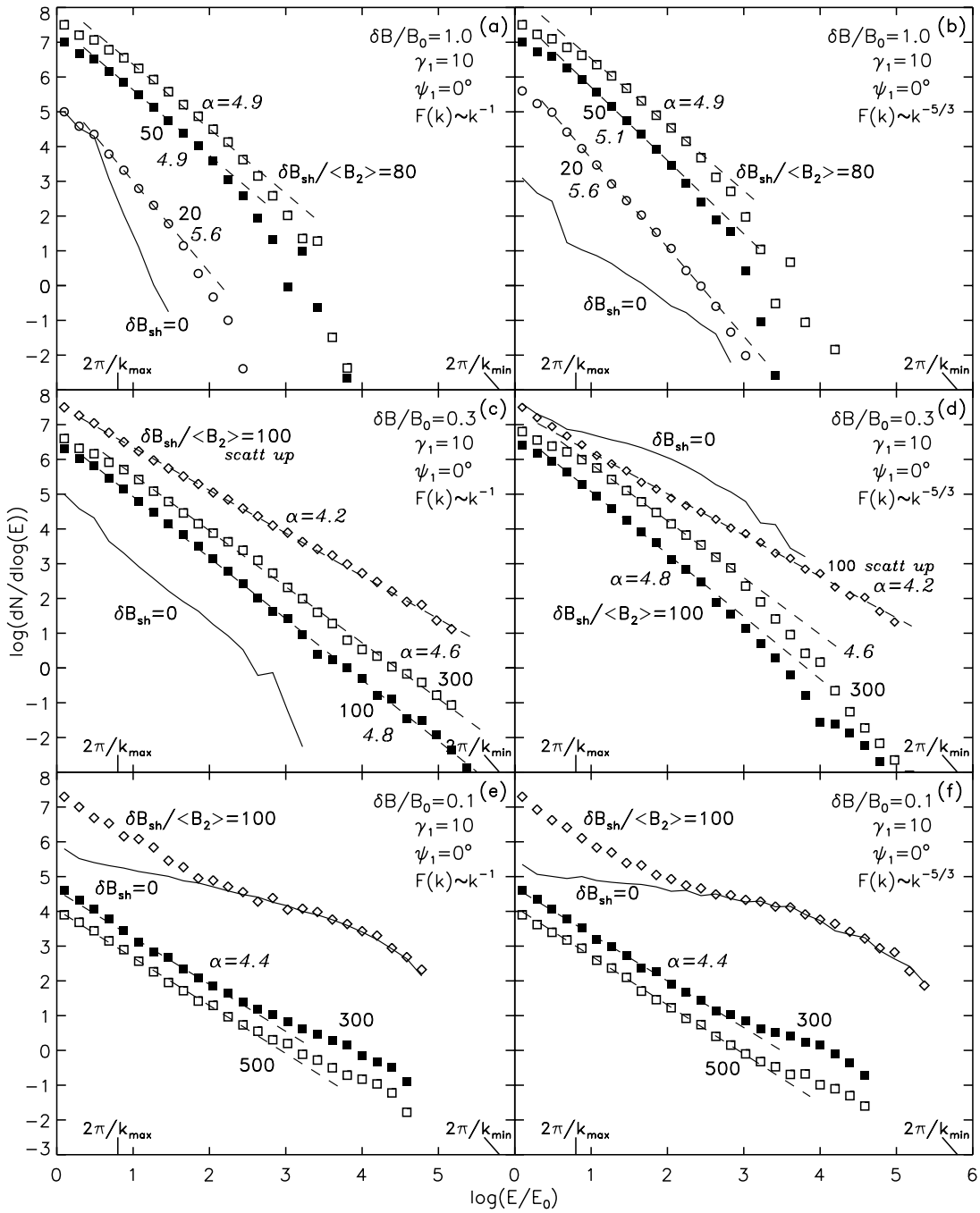

FIG. 6.—Accelerated particle spectra at parallel ultrarelativistic shocks ($\gamma_1 = 10$, $\psi_1 = 0°$). The parameters of the large-scale background magnetic field turbulence structure are provided in each panel. The spectra shown with solid lines have been derived in simulations without small-scale perturbations (see Fig. 4 in Niemiec & Ostrowski 2006). The results indicated as "*scatt up*" in (*c*) and (*d*) show spectra obtained in simulations for which the particle pitch-angle scattering was introduced both downstream and upstream of the shock.

$\delta B_{\rm sh}$. To understand this feature, we have performed additional test simulations with the short-wave component introduced both downstream and *upstream* of the shock (with constant upstream scattering amplitude $\Delta\Omega(E)_{\rm up} = {\rm const} \ll 1/\gamma_1$). As proved earlier in the literature (e.g., Bednarz & Ostrowski 1998; Achterberg et al. 2001; Ellison & Double 2004), this case, equivalent to the pure pitch-angle diffusion model, should lead to the formation of the "universal" spectrum and, indeed, such a spectrum is produced in our simulations (described as "*scatt up*" in Fig. 6*c*). Thus, the slightly steeper spectra obtained in the models with only a downstream short-wave component can be understood solely as the result of the upstream long-wave turbulence providing a different distribution of pitch-angle perturbations to the particle orbits than the purely diffusive process (see Fig. 7). The subsequent generation of a power-law particle spectrum leads to somewhat larger spectral indices than the "universal" value.

With the Kolmogorov wave spectrum (Fig. 6*d*), there is enough power in long waves to influence the particle spectrum at high energies, leading to the noticeable steepening of the particle distributions below $E_{\rm res,max}$. However, in this case as well, the model with the short-wave field perturbations imposed upstream of the shock yields the "universal" power-law spectrum.

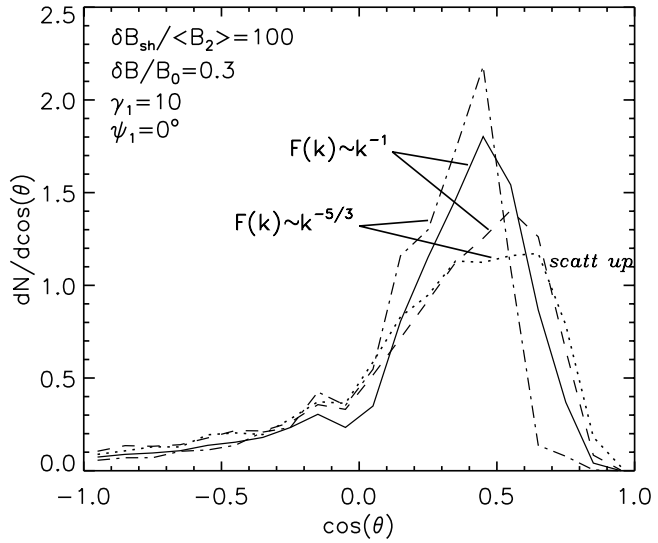

FIG. 7.—Particle angular distributions at parallel shocks ($\gamma_1 = 10$, $\psi_1 = 0^\circ$) for $\delta B_{\rm sh}/\langle B_2\rangle = 100$ and a weakly perturbed large-scale background magnetic field ($\delta B/B_0 = 0.3$) with either the flat (*solid and dashed lines*) or the Kolmogorov (*dash-dotted and dotted lines*) wave power spectrum of magnetic field perturbations. The distributions indicated as "*scatt up*" are derived in a model with short-wave turbulence imposed both downstream and upstream of the shock.

In Figure 7, we compare the angular distributions of particles at the shock in the cases of only downstream small-scale turbulence and with pitch-angle diffusion also imposed upstream of the shock.

The spectra for weakly perturbed background magnetic fields, $\delta B/B_0 = 0.1$, presented in Figures 6*e* and 6*f*, show a new characteristic feature, namely a high-energy spectral bump following the steeper power-law component at lower particle energies. The bump shape closely resembles the distribution of particles accelerated without the shock-generated field component (see the discussion in Niemiec & Ostrowski 2006), and its presence indicates that at these energies the short-wave perturbations become negligible compared to the background long-wave component. Note that $\delta B_{\rm sh}$ is scaled with respect to $\langle B_2\rangle$, which is relatively small here in comparison to the cases with larger $\delta B/B_0$ discussed above.

We have also performed a series of simulations for shocks with a larger Lorentz factor of $\gamma_1 = 30$. The particle spectra presented in Figure 8 for $\delta B_{\rm sh}/\langle B_2\rangle = 100$ show spectral features similar to those observed for shocks with $\gamma_1 = 10$. However, there is an approximate scaling between the two cases, with characteristic spectral features appearing at respectively lower amplitudes of the long-wave magnetic field perturbations $\delta B/B_0$ for shocks with $\gamma_1 = 30$ than in the spectra for $\gamma_1 = 10$. Such a scaling may result from the stronger compression of these perturbations, as measured between the two plasma rest frames, and also from the larger particle anisotropy involved at the higher-γ shock.

4. CONCLUDING REMARKS

The present paper concludes our studies (Niemiec & Ostrowski 2004, 2006) of the first-order Fermi acceleration mechanism acting at relativistic and ultrarelativistic shock waves. We have attempted to consider the most realistic models possible for the perturbed magnetic field structures at the shock, which allow us to study all the field characteristics important for particle acceleration. In particular, we have investigated the dependence of particle spectra on the mean magnetic field inclination with respect to the shock normal and on the power spectra of magnetic field perturbations, including the long-wave background turbulence and the short-wave turbulence generated at the shock.

In this work we append the model of Niemiec & Ostrowski (2006) with a downstream large-amplitude small-scale MHD turbulence component, analogous to those seen in PIC simulations of collisionless relativistic shocks. The form of these additional perturbations is arbitrarily chosen to consist of very short sinusoidal waves that form (static) isotropic highly nonlinear turbulence. We have considered a wide variety of ultrarelativistic shock configurations for which, as presented in § 3, a number of different spectral features can be observed. We show that with growing particle energy, the role of short-wave [$\lambda_{\rm sh} \ll r_g(E)$] magnetic field perturbations decreases, and spectra at high energies are shaped only by the mean magnetic field and the long-wave perturbations. Thus, in oblique superluminal shocks, concave particle spectra with cutoffs can be generated even for $\delta B_{\rm sh} \gg \langle B_2\rangle$. Extended power-law particle distributions can be formed in parallel shocks propagating in a medium with

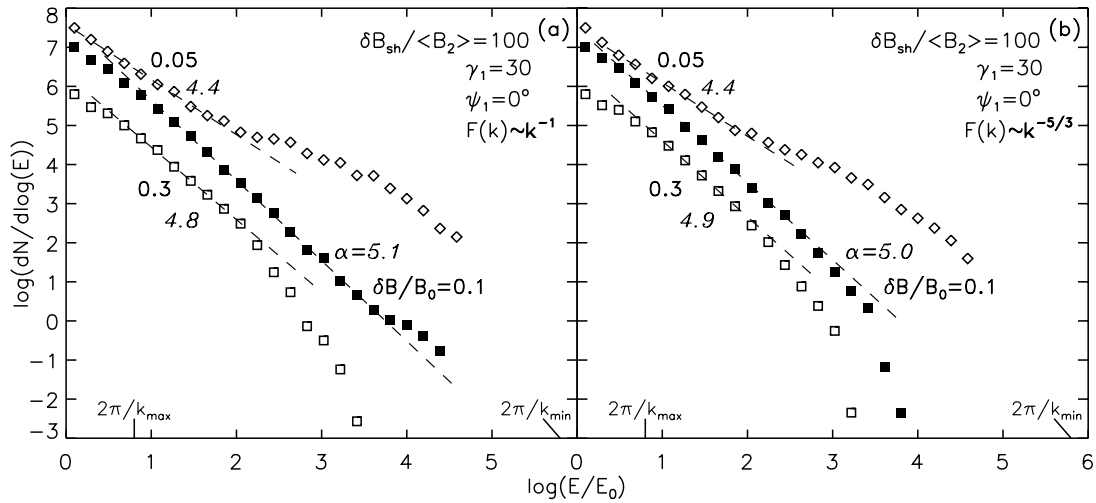

FIG. 8.—Particle spectra at parallel ($\psi_1 = 0^\circ$) ultrarelativistic shocks with $\gamma_1 = 30$, derived for a high amplitude of downstream short-wave perturbations $\delta B_{\rm sh}/\langle B_2\rangle = 100$, and (*a*) the flat and (*b*) the Kolmogorov wave-power spectrum of large-scale background magnetic field turbulence. The amplitudes of the background perturbations $\delta B/B_0$ are given near the respective results, together with the values of the spectral indices fitted to the power-law portions of the spectra.

low-amplitude long-wave field perturbations, but the spectral indices obtained are larger than the "universal" spectral index $\alpha_u \approx 4.2$ that is widely considered in the literature. The only case in which we have been able to obtain spectra with $\alpha = \alpha_u$ involved the unphysical assumption of a constant pitch-angle scattering term upstream of the shock.

In summary, the accelerated particle spectral distributions obtained in this work and in our previous studies (Niemiec & Ostrowski 2004, 2006) generally differ from the spectra of relativistic electrons (power-laws with the spectral indices close to α_u) inferred from modeling of the electromagnetic emission spectra in astrophysical sources hosting relativistic shocks (e.g., hot spots in extragalactic radio sources, quasar jets, gamma-ray burst afterglows). Our results thus provide a strong argument against considering the first-order Fermi shock acceleration as the main mechanism producing the observed radiating electrons. In our opinion, other processes must be invoked to explain the observed emission spectra, for example, the second-order Fermi process acting in the regions of relativistic MHD turbulence downstream of the shock, which has hardly ever been discussed for magnetized relativistic plasmas until now (Virtanen & Vainio 2005), or the collisionless plasma processes that have been studied in numerous PIC simulations (e.g., Hoshino et al. 1992; Hededal et al. 2004; Nishikawa et al. 2006), or even other nonstandard acceleration processes such as those discussed by Stern (2003) for electrons or Derishev et al. (2003) for both electrons and protons.

Our simulations also show that relativistic shocks, being essentially always superluminal, possibly generate accelerated particle distributions with cutoffs either below the maximum resonance energy enabled by the *high-amplitude* background turbulence [$r_g(E_{\rm cutoff}) < \lambda(E_{\rm res,max})$] or approximately at the energy of the compressed background plasma ions $E_{\rm cutoff} \sim \gamma_1 m_i c^2$ (where m_i is a mass of the heaviest ions present in the background medium). Thus, in conclusion, we maintain our opinion from the previous publications (see also Begelman & Kirk 1990) that relativistic shocks are not promising sites as possible sources of ultra-high-energy cosmic rays registered by air shower experiments.

We are grateful to Mikhail Medvedev for interesting discussions. The present work was supported by MNiI during the years 2005–2008 as research project 1 P03D 003 29.

REFERENCES

Achterberg, A., Gallant, Y. A., Kirk, J. G., & Guthmann, A. W. 2001, MNRAS, 328, 393
Bednarz, J., & Ostrowski, M. 1996, MNRAS, 283, 447
———. 1998, Phys. Rev. Lett., 80, 3911
Begelman, M. C., & Kirk, J. G. 1990, ApJ, 353, 66
Derishev, E. V., Aharonian, F., Kocharovsky, V. V., Kocharovsky, Vl. V. 2003, Phys. Rev. D, 68, 043003
Ellison, D. C., & Double, G. P. 2002, Astropart. Phys., 18, 213
———. 2004, Astropart. Phys., 22, 323
Frederiksen, J. T., Hededal, C., Haugbølle, T., & Nordlund, Å. 2004, ApJ, 608, L13
Gallant, Y. A., & Achterberg, A. 1999, MNRAS, 305, L6
Heavens, A., & Drury, L. O'C. 1988, MNRAS, 235, 997
Hededal, C., Haugbølle, T., Frederiksen, J. T., & Nordlund, Å. 2004, ApJ, 617, L107
Hededal, C., & Nishikawa, K.-I. 2005, ApJ, 623, L89
Hoshino, M., Arons, J., Gallant, Y. A., & Langdon, A. B. 1992, ApJ, 390, 454
Jaroschek, C. H., Lesch, H., & Treumann, R. A. 2005, ApJ, 618, 822
Keshet, U., & Waxman, E. 2005, Phys. Rev. Lett., 94, 111102
Kirk, J. G., Guthmann, A. W., Gallant, Y. A., & Achterberg, A. 2000, ApJ, 542, 235
Kirk, J. G., & Heavens, A. 1989, MNRAS, 239, 995
Kirk, J. G., & Schneider, P. 1987, ApJ, 315, 425
Lemoine, M., & Pelletier, G. 2003, ApJ, 589, L73
Medvedev, M. V., & Loeb, A. 1999, ApJ, 526, 697
Niemiec, J., & Ostrowski, M. 2004, ApJ, 610, 851
———. 2006, ApJ, 641, 984
Nishikawa, K.-I., Hardee, P., Hededal, C., & Fishman, G. J. 2006, ApJ, 642, 1267
Nishikawa, K.-I., Hardee, P., Richardson, G., Preece, R., Sol, H., & Fishman, G. J. 2003, ApJ, 595, 555
———. 2005, ApJ, 622, 927
Ostrowski, M. 1991, MNRAS, 249, 551
———. 1993, MNRAS, 264, 248
Ostrowski, M., & Bednarz, J. 2002, A&A, 394, 1141
Silva, L. O., Fonseca, R. A., Tonge, J. W., Dawson, J. M., Mori, W. B., & Medvedev, M. V. 2003, ApJ, 596, L121
Stern, B. E. 2003, MNRAS, 345, 590
Virtanen, J., & Vainio, R. 2005, ApJ, 621, 313